RSC Advances

COMMUNICATION

View Article Online
View Journal | View Issue

Cite this: *RSC Adv.*, 2015, **5**, 8307

Received 23rd October 2014
Accepted 23rd December 2014

DOI: 10.1039/c4ra12988a

www.rsc.org/advances

Novel PtO decorated MWCNTs as a highly efficient counter electrode for dye-sensitized solar cells†

Xiao Chen,‡[a] Jian Wei Guo,‡[a] Yu Hou,[a] Yu Hang Li,[a] Shuang Yang,[a] Li Rong Zheng,[c] Bo Zhang,[a] Xiao Hua Yang*[a] and Hua Gui Yang[ab]

PtO decorated multi-walled carbon nanotubes (MWCNTs) were prepared by a polymer ligand assisted strategy and applied as the counter electrode (CE) in dye-sensitized solar cells (DSCs) for the first time. Compared with the energy conversion efficiency (E_{ff}) of Pt CE based DSCs, the DSCs with PtO–MWCNTs CE showed an overall E_{ff} of 8.67%, giving an improvement of 12.7%. Better electrocatalytic activity towards I_3^-/I^- redox pairs than Pt CE indicated that the PtO–MWCNTs was a promising electrocatalyst for DSCs.

The dye-sensitized solar cells (DSCs) were first reported by O'Regan and Grätzel in 1991 and have become the focus of attention for their low consumption, easy fabrication and powerful harvesting efficiency.[1] As one of the most important components in DSCs, the counter electrode (CE) collects the electrons from the external circuit, and catalyzes the reduction of triiodide ions.[2] It is well-known that platinum is a superior CE material due to its excellent catalytic activity for I_3^- reduction and high electrical conductivity. However, the high price and low reserve of Pt severely restrict the large-scale application of the DSCs.[3] Therefore, many efforts have been devoted to exploring low-cost and high performance materials as replacements for Pt, such as different forms of carbon materials,[4] conducting polymers,[5] metal sulphides,[6] metal carbides,[7] metal nitrides,[8] metal phosphides[9] and metal oxides.[10] Among these developed substitutes, Pt decorated multi-walled carbon nanotubes (MWCNTs) are well researched and demonstrate better electrocatalytic activity for I_3^-/I^- redox reaction than that of Pt.[11] Recently, the PtO was reported to be an excellent catalyst for photocatalytic hydrogen evolution.[12] To the best of our knowledge, there is no report about the PtO decorated MWCNTs as CE in DSCs.

Here, we utilize a trithiol-terminated poly(methacrylic acid) synthesize PtO–MWCNTs nanocomposite, and apply it as CE materials in DSCs. The chemical state of Pt species on the surface of MWCNTs was confirmed to be Pt^{2+} by extended X-ray absorption fine structure (EXAFS) and X-ray photoelectron spectroscopy (XPS) measurements. Moreover, the PtO–MWCNTs CE based solar cells yield an energy conversion efficiency of 8.67%, giving an improvement of 12.7% than that of Pt CE. Better electrocatalytic activity of PtO–MWCNTs indicates that the PtO–MWCNTs nanocomposite is a promising catalyst in DSCs.

The overall morphology of PtO–MWCNTs nanocomposites was analyzed using the transmission electron microscopy (TEM). As shown in Fig. 1A, the PtO nanoparticles are dispersed homogeneously on the surface of MWCNTs with ultra-small particle size. The size distribution image in Fig. 1D confirms that PtO nanoparticles with mainly a size range of 0.8–1.0 nm are dispersedly loaded on the surface of the MWCNTs. The elemental analysis of the PtO–MWCNTs nanocomposites, employing energy dispersive spectroscopy (EDS) (Fig. 1C), reveals that elements of Pt, O and C coexisted in the sample, which demonstrates that the composite prepared by our strategy is composed of oxidized Pt and MWCNTs. Fig. 1B shows the enlarged HR-TEM image of the PtO loaded on the MWCNTs surface. The lattice distance in the enlarged view was measured to be 0.218 nm, corresponding to the {110} surface of PtO. The scanning electron microscopy (SEM) images of prepared PtO–MWCNTs CE and Pt CE on FTO are shown in Fig. S3.†

In order to further examine the chemical state of Pt species on the surface of MWCNTs, the PtO–MWCNTs nanocomposites were then studied by EXAFS and XPS measurements. Fig. 2A shows that only one apparent peak at 1.0–2.0 Å is displayed in Fourier-transformed spectrum of EXAFS for the PtO–MWCNTs. To identify the nature of the backscatter, EXAFS spectra of Pt

[a]*Key Laboratory for Ultrafine Materials of Ministry of Education, School of Materials Science and Engineering, East China University of Science and Technology, 130 Meilong Road, Shanghai, China 200237. E-mail: yangxh@ecust.edu.cn; Fax: +86-21-6425-2127; Tel: +86-21-6425-2127*

[b]*Centre for Clean Environment and Energy, Griffith University, Gold Coast Campus, Queensland 4222, Australia*

[c]*Beijing Synchrotron Radiation Facility, Institute of High Energy Physics, Chinese Academy of Sciences, Beijing 100049, China*

† Electronic supplementary information (ESI) available. See DOI: 10.1039/c4ra12988a

‡ These authors contributed equally to this work.

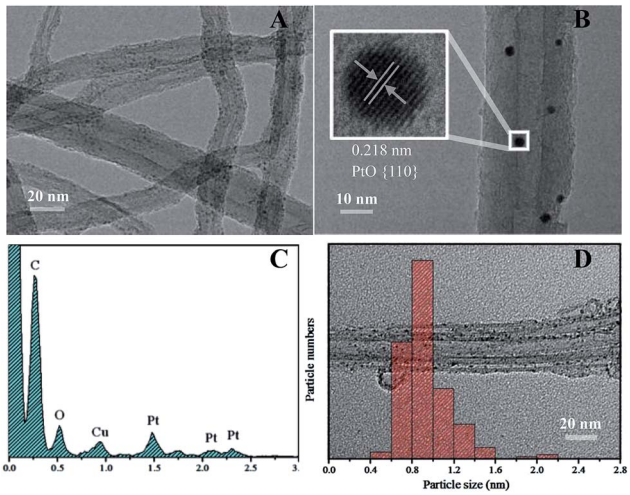

Fig. 1 (A) HR-TEM image of PtO–MWCNTs nanocomposites, (B) the enlarged view of the HR-TEM image of the PtO loaded on the MWCNTs surface, (C) EDS spectrum of the synthesized PtO–MWCNTs nanocomposites, (D) size distribution of PtO nanoparticles loaded on the MWCNTs (based on a count of 197 nanocrystallites).

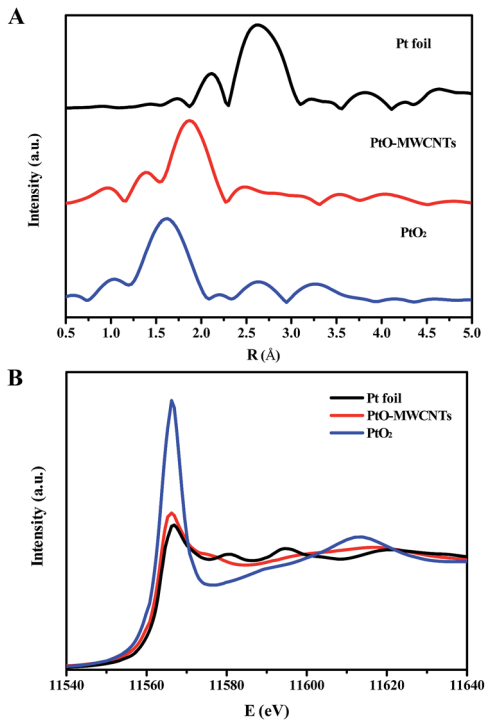

Fig. 2 (A) The k^3-weighted Fourier transform spectra from EXAFS, ×1/3 represents signal magnification, (B) the normalized X-ray absorption near-edge structure spectra at the Pt L_3-edge of the Pt foil, PtO_2 and initial PtO–MWCNTs.

and PtO_2 samples were measured as reference. The peak at 1.0–2.0 Å in PtO_2 is due to scattering from the nearest oxygen atoms, whereas the peak at 2.0–3.3 Å in Pt foil is related to scattering from the neighbouring Pt. Thus, the only peak at 1.0–2.0 Å in PtO–MWCNTs is believed to be the contribution from Pt–O binding. Fig. 2B shows the normalized X-ray absorption near-edge structure spectrum of PtO–MWCNTs, and the reference spectra of Pt foil and PtO_2. The intensities in the spectra reflect the oxidation state of Pt in different samples. Thus, the intensity of the PtO–MWCNTs, which is between that of Pt and PtO_2, further suggests that the Pt in the materials exists as oxidized Pt.[13] The X-ray photoelectron spectroscopy (XPS; Fig. S1†) was further studied to examine the chemical state of Pt species in obtained materials. The main peaks in PtO–MWCNTs centre at 72.8 and 76.0 eV, which can be assigned to Pt^{2+} bonded to oxygen.[14]

Fig. 3 shows the photocurrent–voltage (J–V) curves of the DSCs with different CEs measured under illumination at 100 mW cm^{-2} and the detailed photovoltaic parameters are summarized in Table 1. As shown in Fig. 3, higher J_{sc} (17.93 mA cm^{-2}) of PtO–MWCNTs CE based DSCs indicates that PtO–MWCNTs CE demonstrates better electrocatalytic activity for I_3^- reduction than that of Pt CE.[15] Moreover, the V_{oc} (763.6 mV) of PtO–MWCNTs CE based DSC is higher than that of Pt CE (746.2 mV), which means there are more interfacial active sites in PtO–MWCNTs CE.[16] Compared with the E_{ff} (7.69%) of Pt CE based solar cells, the DSCs with PtO–MWCNTs CE show an overall E_{ff} of 8.67%, giving an improvement of 12.7%.

In order to further investigate the different catalytic activity for triiodide reduction between the PtO–MWCNTs CEs and Pt CEs, the electrochemical impedance spectroscopy (EIS) measurement was employed and the Nyquist plots of the symmetrical cells were shown in Fig. 4. The values of the series resistance (R_s), the charge-transfer resistance (R_{ct}) and constant phase element (CPE) are obtained by fitting the spectra with an EIS spectrum analyzer, and summarized in Table 1. The equivalent circuit used to fit the experimental EIS data is shown in the inset of Fig. 4. The R_s is mainly composed of the bulk resistance of CEs materials, resistance of FTO glass substrate and contact resistance, *etc.* The R_s of PtO–MWCNTs CEs is 9.41 Ω, while this value of Pt CEs is 11.42 Ω. A relatively faster electron transfer kinetics and better electrical conductivity are responsible for the decrease in R_s of the

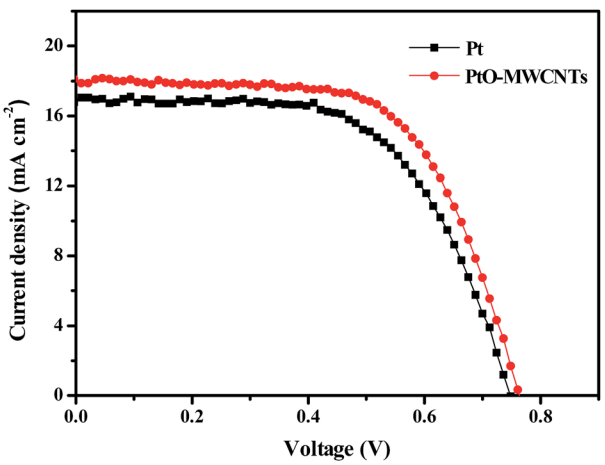

Fig. 3 J–V characteristics of the DSCs with Pt CE and PtO–MWCNTs CE measured at 100 mW cm^{-2}.

Table 1 Photovoltaic parameters of DSCs with different counter electrodes, measured at 100 mV cm^{-2} illumination

CE sample	J_{sc} mA cm^{-2}	V_{oc} mV	FF%	η%	R_s Ω	R_{ct} Ω	C μF
Pt	16.95	746.2	60.8	7.69	11.42	2.66	2.42
PtO–MWCNTs	17.93	763.6	63.3	8.67	9.41	0.78	109.6

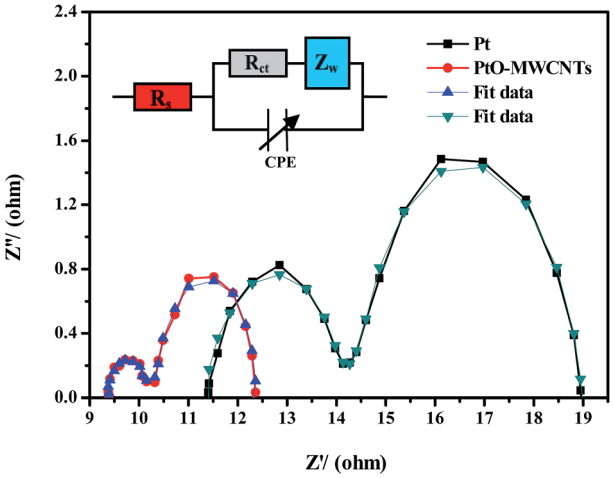

Fig. 4 EIS curves of the DSCs with Pt CE and PtO–MWCNTs CE, measured at 100 mW cm^{-2} light intensity.

PtO–MWCNTs CEs.[10a] The R_{ct} is a measure of the ease of electron exchange between the counter electrode and the electrolyte and thus varies inversely with the triiodide reduction activity of the CEs. The lower R_{ct} of PtO–MWCNTs leads to a better catalytic activity, explaining the better performance than that of Pt CEs based cells.[17] Moreover, a much larger capacitance (C) of PtO–MWCNTs CE indicates a higher surface area than that of Pt CE, which is responsible for higher E_{ff} and in agreement with previous report.[16] In conclusion, low R_s, low R_{ct} and high C result in the high power-conversion efficiency of DSCs with PtO–MWCNTs CE and agree well with the photovoltaic experiments.

To further examine the interfacial charge-transfer properties of the triiodide/iodide couple in the electrode surface, Tafel polarization measurement was carried out with dummy cells fabricated with two identical electrodes (CE//electrolyte//CE). The Tafel curves in Fig. S2† show that the current density (J) is a logarithmic function of the voltage (U). In Tafel zone (at middle overpotential), the anodic and cathodic branches of the PtO–MWCNTs CE show a larger slope than the conventional Pt CE, indicating the presence of a large exchange current density on the electrode surfaces, which means that PtO–MWCNTs CE has a higher catalytic activity than the Pt CE. Moreover, the current densities of PtO–MWCNTs CE obtained in all three zones are higher, which is consistent with the results of photovoltaic and EIS measurements.[17]

The cyclic voltammetry (CV) measurement was further carried out in a three-electrode system to evaluate the

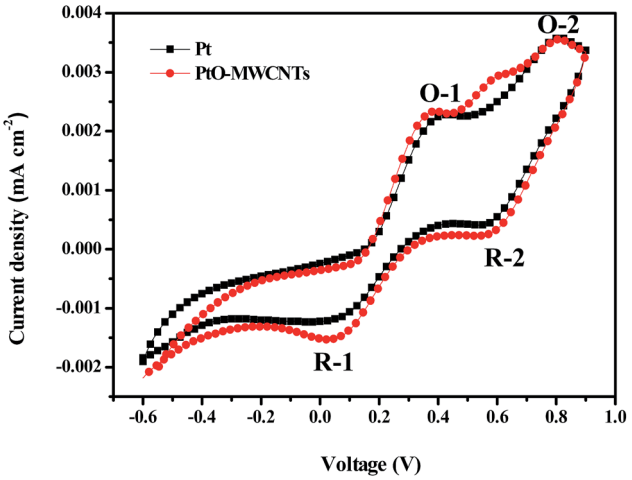

Fig. 5 Cyclic voltammograms of iodide species for PtO–MWCNTs and Pt electrodes.

electrocatalytic properties of the PtO–MWCNTs CE (Fig. 5). Typical curves with two pairs of oxidation and reduction peaks (O-1/R-1, O-2/R-2) are obtained for PtO–MWCNTs CE. The left peak is corresponding to the redox reaction of eqn (1), while the right one is corresponding to the reaction of eqn (2).

$$I_3^- + 2e = 3I^- \quad (1)$$

$$3I_2 + 2e = 2I_3^- \quad (2)$$

As shown in Fig. 5, the CEs based on the PtO–MWCNTs and Pt show very similar shapes in terms of redox peak positions. Comparing the current densities of two CEs, PtO–MWCNTs nanocomposites exhibit higher values than that of Pt, suggesting a higher intrinsic catalytic activity for redox reaction of iodide ions.[18] Moreover, the peak-to-peak splitting (E_{pp}) of PtO–MWCNTs CE is slightly smaller than that of bare Pt CE, further conforming that the electrocatalytic activity and reversibility of I_3^-/I^- redox reaction on PtO–MWCNTs CE are better.[6]

In summary, we demonstrate a PMAA–PTTM polymer ligands assisted method to synthesize PtO–MWCNTs nanocomposites. The chemical state of Pt species in the PtO–MWCNTs nanocomposite is confirmed to be Pt^{2+} by EXAFS and XPS measurements. Furthermore, PtO–MWCNTs CE exhibits better photovoltaic performance than the conventional Pt electrode, which indicates PtO–MWCNTs is a high-efficient CE material for DSCs.

Acknowledgements

This work was financially supported by National Natural Science Foundation of China (21373083, 21203061), Fundamental Research Funds for the Central Universities (WD1313009, WD1214036, WM1314018), Shanghai Municipal Natural Science Foundation (14ZR1410200) and China Postdoctoral Science Foundation (2013T60425).

Notes and references

1 (*a*) B. O'Regan and M. Grätzel, *Nature*, 1991, **353**, 737–740; (*b*) M. Grätzel, *Nature*, 2001, **414**, 338–344.
2 (*a*) G. R. Li, F. Wang, Q. W. Jiang, X. P. Gao and P. W. Shen, *Angew. Chem., Int. Ed.*, 2010, **49**, 3653–3656; (*b*) H. Zhang, Y. Wang, D. Yang, Y. Li, H. Liu, P. Liu, B. J. Wood and H. Zhao, *Adv. Mater.*, 2012, **24**, 1598–1603.
3 K. C. Huang, Y. C. Wang, R. X. Dong, W. C. Tsai, K. W. Tsai, C. C. Wang, Y. H. Chen, R. Vittal, J. J. Lin and K. C. Ho, *J. Mater. Chem.*, 2010, **20**, 4067–4073.
4 (*a*) P. Joshi, Y. Xie, M. Ropp, D. Galipeau, S. Bailey and Q. Q. Qiao, *Energy Environ. Sci.*, 2009, **2**, 426–429; (*b*) L. Kavan, J. H. Yum and M. Grätzel, *ACS Nano*, 2011, **5**, 165–172.
5 S. Ahmad, J. H. Yum, H. J. Butt, M. K. Nazeeruddin and M. Grätzel, *ChemPhysChem*, 2010, **11**, 2814–2819.
6 (*a*) M. Wang, A. M. Anghel, B. T. Marsan, N. L. Cevey Ha, N. Pootrakulchote, S. M. Zakeeruddin and M. Grätzel, *J. Am. Chem. Soc.*, 2009, **131**, 15976–15977; (*b*) X. Chen, Y. Hou, B. Zhang, X. H. Yang and H. G. Yang, *Chem. Commun.*, 2013, **49**, 5793–5795.
7 M. Wu, X. Lin, A. Hagfeldt and T. Ma, *Angew. Chem., Int. Ed.*, 2011, **50**, 3520–3524.
8 A. M. Hung, N. A. Konopliv and J. N. Cha, *Langmuir*, 2011, **27**, 12322–12328.
9 M. Wu, J. Bai, Y. Wang, A. Wang, X. Lin, L. Wang, Y. Shen, Z. Wang, A. Hagfeldt and T. Ma, *J. Mater. Chem.*, 2012, **22**, 11121–11127.
10 (*a*) Y. Hou, D. Wang, X. H. Yang, W. Q. Fang, B. Zhang, H. F. Wang, P. Hu, H. J. Zhao and H. G. Yang, *Nat. Commun.*, 2014, **4**, 1583; (*b*) L. Cheng, Y. Hou, B. Zhang, S. Yang, J. W. Guo, L. Wu and H. G. Yang, *Chem. Commun.*, 2013, **49**, 5945–5947.
11 (*a*) L.-Y. Chang, C.-P. Lee, K.-C. Huang, Y.-C. Wang, M.-H. Yeh, J.-J. Lin and K.-C. Ho, *J. Mater. Chem.*, 2012, **22**, 3185–3191; (*b*) G. Eda, H. Yamaguchi, D. Voiry, T. Fujita, M. Chen and M. Chhowalla, *Nano Lett.*, 2011, **11**, 5111–5116.
12 Y. H. Li, J. Xing, Z. J. Chen, Z. Li, F. Tian, L. R. Zheng, H. F. Wang, P. Hu, H. J. Zhao and H. G. Yang, *Nat. Commun.*, 2014, **4**, 2500.
13 R. K. Nomiyama, M. J. Piotrowski and J. L. F. Da Silva, *Phys. Rev. B: Condens. Matter Mater. Phys.*, 2011, **84**, 100101.
14 J. Xing, H. B. Jiang, J. F. Chen, Y. H. Li, L. Wu, S. Yang, L. R. Zheng, H. F. Wang, P. Hu, H. J. Zhao and H. G. Yang, *J. Mater. Chem. A*, 2013, **48**, 15258–15264.
15 L. X. Yi, Y. Y. Liu, N. L. Yang, Z. Y. Tang, H. J. Zhao, G. H. Ma, Z. G. Su and D. Wang, *Energy Environ. Sci.*, 2013, **6**, 835–840.
16 X. Chen, Y. Hou, S. Yang, X. H. Yang and H. G. Yang*J. Mater. Chem. A*, 2014, **2**, 17253–17257.
17 J. W. Guo, B. Zhang, Y. Hou, S. Yang, X. H. Yang and H. G. Yang, *J. Mater. Chem. A*, 2013, **1**, 1982–1986.
18 (*a*) F. Pichot and B. A. Gregg, *J. Phys. Chem. B*, 1999, **104**, 6–10; (*b*) H. C. Sun, Y. H. Luo, Y. D. Zhang, D. M. Li, Z. X. Yu, K. X. Li and Q. B. Meng, *J. Phys. Chem. C*, 2010, **114**, 11673–11679; (*c*) H. H. Niu, S. X. Qin, X. L. Mao, S. W. Zhang, R. B. Wang, L. Wan, J. Z. Xu and S. D. Miao, *Electrochim. Acta*, 2014, **121**, 285–293.

